Pulsed EPR Characterization of the Low-Spin Iron(III) Porphyrinate Complexes with Phenyl Isocyanide Ligands Having the d_{xy} Orbital Ground State

Andrei V. Astashkin,* Arnold M. Raitsimring, Abigail R. Kennedy, Tatjana Kh. Shokhireva, and F. Ann Walker

Department of Chemistry, University of Arizona, Tucson, Arizona 85721-0041

Received: August 8, 2001

Pulsed electron−nuclear double resonance and electron spin−echo envelope modulation spectroscopies have been used to characterize the bis(phenyl isocyanide) complexes of iron(III)-tetraphenylporphyrin ([TPPFe-(PhNC)$_2$]$^+$) and iron(III)-octaethylporphyrin ([OEPFe(PhNC)$_2$]$^+$) that have the d_{xy} orbital configuration. The spin density distribution in the porphyrin π system was obtained, with major spin density ($\sim$0.06) being delocalized to each *meso* carbon atom. The spin density on the pyrrole β carbons was found to be negligible. The upper limit for spin density on Fe^{3+} was estimated to be about 0.63. The hyperfine interaction constants on the pyrrole nitrogens (on average, $\sim$3.3 MHz) were also evaluated. The overall spin density distribution obtained was found to be in agreement with that estimated theoretically (Ghosh, A.; Gonzalez, E.; Vangberg, T. *J. Phys. Chem. B* **1999**, *103*, 1363) using density functional theory.

Introduction

Over the past twelve years, we and other researchers have shown that low-spin Fe(III) porphyrinates may have two different electronic ground states, either that for which the electron configuration is $(d_{xy})^2(d_{xz},d_{yz})^3$ and the unpaired electron is in the d_π orbitals[1−7] or that for which the electron configuration is $(d_{xz},d_{yz})^4(d_{xy})^1$ and the unpaired electron is in the d_{xy} orbital[2,8−17] (the molecular axes *X* and *Y* are in the porphyrin plane, along the mutually perpendicular Fe−N directions, and *Z* is normal to the plane). The former electronic ground state is observed in Fe(III) porphyrinates having imidazoles or high-basicity pyridines as axial ligands,[1−7] whereas the latter is found in iron(III) porphyrinates having low-basicity pyridines or isocyanides as axial ligands,[8−11] as well as in the cyanide complexes of several synthetic iron porphyrinates,[12−17] and in low-spin sirohem, an iron(III) isobacteriochlorin complex, which is the active site of sulfite reductase.[18,19] The complexes having the $(d_{xy})^2(d_{xz},d_{yz})^3$ ground state electron configuration typically show either rhombic or "large g_{max}" EPR spectra with the largest principal *g* value corresponding to the direction along *Z*,[1−7] whereas those complexes with the $(d_{xz},d_{yz})^4(d_{xy})^1$ ground-state electron configuration often show axial EPR spectra but, whether axial or rhombic, with the smallest principal *g* value corresponding to the direction along *Z*.[8−11]

The orientation of the *g* tensor in the molecular frame can be determined from single-crystal electron paramagnetic resonance (EPR) experiments using the information on the crystal structures obtained by X-ray crystallography.[20−26] Now, however, it is not always necessary to go to the effort of growing single crystals and performing the X-ray experiments, because of the general availability of modern high-resolution EPR techniques (electron spin−echo envelope modulation (ESEEM) and electron−nuclear double resonance (ENDOR)). Using the orientational selectivity provided by the *g* factor anisotropy, even

in orientationally disordered samples, these techniques can often supply the information on the *g*-tensor orientation and, in addition, give much finer details of the electronic structure of the complexes than the usual continuous wave (CW) EPR experiments on single crystals.[3−7] In the ESEEM studies of bis-pyrazole complexes of TPPFeCl ([TPPFe(PzH)$_2$]$^+$ [3] and [TPPFe-(3-NH$_2$PzH)$_2$]$^+$ [6]), as well as bis-imidazole and bis-(4-dimethylamino)pyridine complexes of OEPFeCl ([OEPFe(ImH)$_2$]$^+$ and [OEP(4-NMe$_2$Py)$_2$]$^+$[4], where TPP and OEP stand for tetraphenylporphyrin and octaethylporphyrin, respectively) and nitrophorin 1-histamine,[5] we have shown that the electron configuration is unambiguously $(d_{xy})^2(d_{xz},d_{yz})^3$, with the unpaired electron residing in the d_{yz} orbital. Recently, we have applied pulsed ENDOR in combination with ESEEM techniques to determine the electronic structure of the bis-imidazole complex of iron(III) tetraphenylchlorin, [TPCFe(ImH)$_2$]$^+$, and showed that this complex also has the $(d_{xy})^2(d_{xz},d_{yz})^3$ ground orbital state.[7]

In this work, ESEEM and pulsed ENDOR spectroscopies are used to characterize the electronic structure of some low-spin ferrihemes with phenyl isocyanide ligands ([TPPFe(PhNC)$_2$]$^+$ and [OEPFe(PhNC)$_2$]$^+$). On the basis of the CW EPR, Mössbauer, and NMR data for closely related complexes,[10,11] the orbital configuration of these complexes is expected to be $(d_{xz},d_{yz})^4(d_{xy})^1$, and our purpose is to obtain as detailed information as possible on the electron spin density distribution in them. To this end, not only have the compounds with natural abundance of isotopes been used, but experiments have also been performed on complexes with ^{2}H-, ^{15}N-, and ^{13}C-labeled phenyl isocyanide ligands.

Experimental Section

The tetraphenylporphyrin free base, TPPH$_2$, was prepared and purified using literature methods.[27,28] Octaethylporphyrin free base was purchased from Midcentury Chemical Co. and used as received. The chloroiron(III) complexes were prepared and purified as described previously.[29] Solutions of the low-spin Fe-(III) porphyrinates ($\sim$5 mM) were prepared in CH$_2$Cl$_2$ or CD$_2$-Cl$_2$, depending on the nuclei of interest in the pulsed EPR

Low-Spin Iron(III) Porphyrinate Complexes

J. Phys. Chem. A, Vol. 106, No. 1, 2002 **75**

experiments (see the figure captions). Excess phenyl isocyanide (4−6 equiv per equivalent of iron porphyrinate) were added to these solutions to ensure complete formation of the bis-isocyanide complex in each case.

Phenyl isocyanide (PhNC or CNPh) was synthesized according to published procedures.[30] Its ^{15}N and ^2H analogues were prepared from the appropriately isotopically labeled precursors ([^{15}N]aniline, d_5-aniline, Cambridge Isotopes). The ^{13}C analogue was prepared from aniline and (^{13}C)formic acid (Cambridge Isotopes) according to literature procedures.[31]

Continuous wave (CW) EPR spectra were measured on a Bruker ESP-300E X-band EPR spectrometer, at 77 K using an immersion dewar. The ESEEM and pulsed ENDOR experiments were carried out on the home-built X/P-band pulsed EPR spectrometer equipped with a pulsed ENDOR accessory.[32,33] In these experiments, the Mims[34] and Davies[35] pulsed ENDOR techniques were employed. To minimize the Mims ENDOR spectrum distortions because of the blind spots,[36,37] the spectra were detected at several time intervals τ between the first and second microwave (mw) pulses of the three-pulse sequence and then summed up. The ^1H ENDOR spectra were also symmetrized with respect to the proton Zeeman frequency in order to enhance the signal-to-noise ratio and minimize the distortions because of the implicit TRIPLE effect.[38]

The antenna-coupled cylindrical resonator for pulsed EPR experiments was put into the flow cryostat CF935 from Oxford Instruments America, Inc. The resonator (38 mm height and 18 mm inner diameter) had a coaxial sapphire ring (12 mm height, 10 mm outer diameter, and 5 mm inner diameter) supported by Teflon inserts, and the Helmholtz radio frequency (RF) coils (2 × 2 turns) were wound through the narrow (0.5 mm diameter) holes bored in the sapphire ring along the central sample hole. This structure has allowed us to place the coils very close to the sample and provided a good isolation of the coil wire from the electric component of the mw field. This probehead had a main resonance at the mw frequency ν_{mw} of about 9.4 GHz. In addition, a resonance zone of higher frequency ($\nu_{mw} \sim 11$ GHz) was present, which has allowed us to perform some of the experiments at different mw frequencies without changing the probehead. The RF amplifier (model 250 L, Amplifier Research) was used in CW and pulsed modes providing the output powers of about 200 and 800 W, respectively. The typical duration of the 180° pulse for protons was about 12 μs when the amplifier was in the CW mode and 8 μs when it was in the pulsed mode. The measurement temperature was about 10 K.

Results

1. EPR Spectra. The X-band CW EPR spectra of [TPPFe-(PhNC)$_2$]$^+$ and [OEPFe(PhNC)$_2$]$^+$ are shown in Figure 1. One can see that these spectra are axial, with the principal g values of $g_{||} = 1.95$ and $g_\perp = 2.20$ for [TPPFe(PhNC)$_2$]$^+$ and $g_{||} = 1.91$ and $g_\perp = 2.25$ for [OEPFe(PhNC)$_2$]$^+$. For the bis-isocyanide complexes, the orbital ground state is $(d_{xz},d_{yz})^4(d_{xy})^1$ and $g_{||} = g_Z$ (i.e., it corresponds to the direction Z).[10,11] Because the g-tensor is (at least, within the X-band EPR resolution) axially symmetric, the directions of the two axes corresponding to $g_\perp$ in the heme plane are arbitrary, and we may take them to be parallel to X and Y.

In the following, the ENDOR and ESEEM results are described for various types of nuclei in [TPPFe(PhNC)$_2$]$^+$ and [OEPFe(PhNC)$_2$]$^+$, obtained at different positions in the EPR spectra. For axial g tensors such as those of the bis-isocyanide complexes of Fe(III) porphyrins,[10,11] different values of the
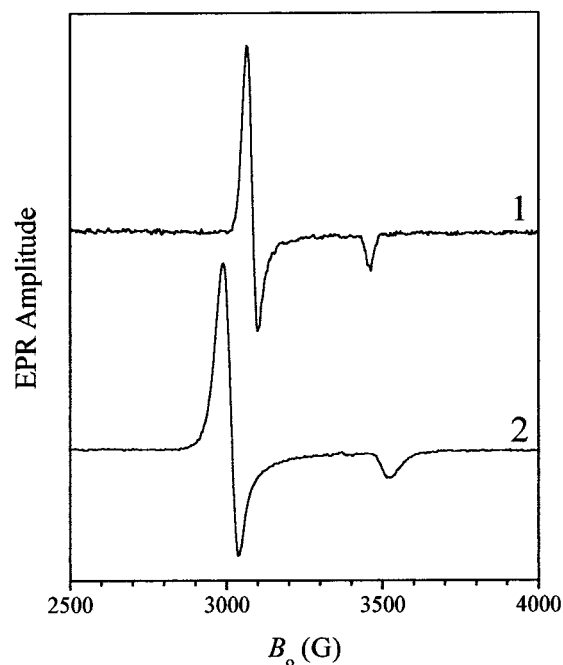

Figure 1. EPR spectra of [TPPFe(PhNC)$_2$]$^+$ (trace 1) and [OEPFe-(PhNC)$_2$]$^+$ (trace 2) in CD$_2$Cl$_2$. Experimental conditions: mw frequency, 9.435 GHz in trace 1 and 9.455 GHz in trace 2; modulation amplitude, 5 G; modulation frequency, 100 kHz; mw power, 2 μW; temperature, 77 K.

observation magnetic field $\boldsymbol{B}_0$ correspond to different angles θ_{BZ} between the $\boldsymbol{B}_0$ vector and the main axis of the g tensor that coincides with the molecular axis Z (hence the notation for the angle):

$$\cos^2 \theta_{BZ} = \frac{g_\perp{}^2 - g^2}{g_\perp{}^2 - g_{||}{}^2} \tag{1}$$

where g is the g value corresponding to a given $\boldsymbol{B}_0$.

2. Protons in the *meso* Positions. When a low-spin Fe(III) porphyrinate has the d_{xy} unpaired electron configuration, the porphyrin macrocycle is strongly ruffled.[9−11] This provides a nonzero overlap between the d_{xy} orbital and the π orbitals of the pyrrole nitrogens.[9] The spin density is thus delocalized into the porphyrin π system, and the d_{xy} orbital effectively becomes a part of the π system. The NMR measurements of such systems show an appreciable spin density on the *meso* carbons.[8−11] Density functional theoretical (DFT) calculations also predict a noticeable spin density on the *meso* carbons but about zero spin density on the pyrrole β carbons.[39]

The π-spin density on the *meso* carbons in the porphyrin ring can be assessed through the measurement of the hyperfine interactions (hfi) of the protons in these positions in the OEP complex. Figure 2a shows the ENDOR spectra of [OEPFe-(PhNC)$_2$]$^+$ taken at various positions in the EPR spectrum of this complex. The angles θ_{BZ} between $\boldsymbol{B}_0$ and Z corresponding to the measurement positions are shown in the figure. The spectra consist of intense lines at the frequencies close to the ^1H Zeeman frequency, ν_H, and weaker lines (aa') with considerably greater splitting. The latter lines are narrow and intense near $g_{||}$ but become progressively broader and weaker as $\boldsymbol{B}_0$ approaches $g_\perp$ region of the EPR spectrum.

In the ENDOR spectra of [OEPFe(PhNC)$_2$]$^+$ with CNPh-d_5, only the central intense lines with splittings less than 1.5 MHz were affected by the H → D isotopic substitution (see below). However, the lines aa' were still observed (see Figure 3a), which

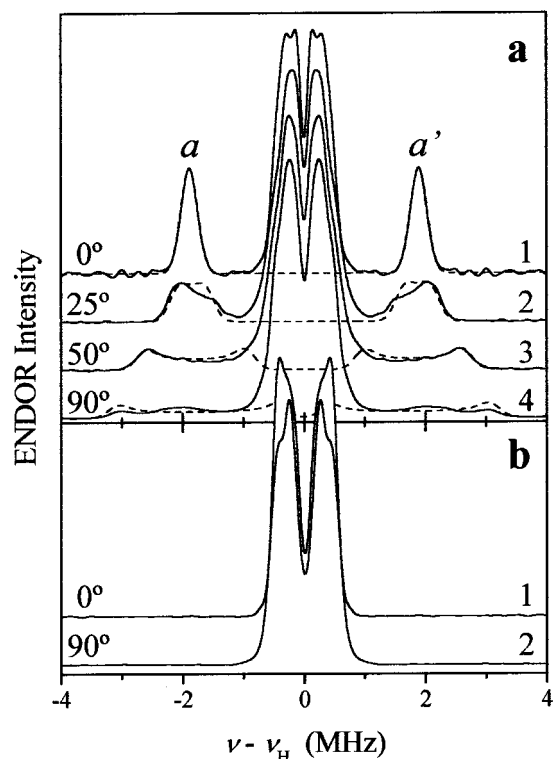**Figure 2.** (a) Solid traces 1 through 4, experimental ^1H Mims ENDOR spectra of $[OEPFe(PhNC)_2]^+$ in CD_2Cl_2, detected at $\nu_{mw} = 9.44$ GHz and at $B_0 = 3550, 3425, 3175,$ and 2985 G, respectively. The corresponding approximate values of θ_{BZ} are shown near each trace at the left-hand side of the figure. Other experimental parameters: mw pulses, $3 \times (10$ ns); time interval between the second and third mw pulses, $T = 30$ μs; RF pulse duration (180°), 12 μs. The presented traces are obtained by summation of spectra recorded at $\tau = 300, 375, 450,$ and 525 ns and symmetrization of the result with respect to the ^1H Zeeman frequency ν_H. Dashed lines are ENDOR spectra simulated for $\rho_{Fe} = 0.63$ and $\rho_{Cm} = 0.06$ (see text). Because the experimental spectra represented sums over several τ values, the ENDOR spectra were calculated without taking into account the Mims ENDOR intensity factor[34] $1 - \cos(2\pi A\tau)$, where A is the hfi constant. (b) Experimental ^1H Mims ENDOR spectra of $[TPPFe(PhNC)_2]^+$ in CD_2Cl_2, detected at $\nu_{mw} = 9.413$ GHz and at $B_0 = 3435$ (trace 1) and 3060 G (trace 2). The corresponding approximate values of θ_{BZ} are shown near each trace at the left-hand side of the figure. Other experimental parameters: mw pulses, $3 \times (10$ ns); time interval between the second and third mw pulses, $T = 30$ μs; RF pulse duration (180°), 12 μs. The presented traces are obtained by summation of spectra recorded at $\tau = 300$ and 375 ns and symmetrization of the result with respect to ν_H.

allows one to conclude that they belong to porphyrin protons. This conclusion is also supported by the fact that no lines corresponding to large hfi constants (greater than 1.5 MHz) are seen in the spectra of $[TPPFe(PhNC)_2]^+$ (see Figure 2b). The TPP complex has the same axial ligands, but its porphyrin ring has phenyl groups instead of protons at the *meso* positions, and protons instead of ethyl groups at pyrrole β carbons. Because, as we mentioned above, only *meso* carbons (of all of the porphyrin atoms attached to protons) are expected to have an appreciable π-spin density, the lines aa' are readily assigned to the porphyrin protons at the meso positions.

The latter conclusion could also be reached independently, on the basis of the ENDOR data presented herein. Indeed, if the protons responsible for the aa' doublet were those of the ethyl groups, then the observed characteristic anisotropy in the line positions (on the order of 3 MHz) would require a very unreasonable spin density of about 0.4 at least for some of the pyrrole β carbons. In $[TPPFe(PhNC)_2]^+$, the characteristic
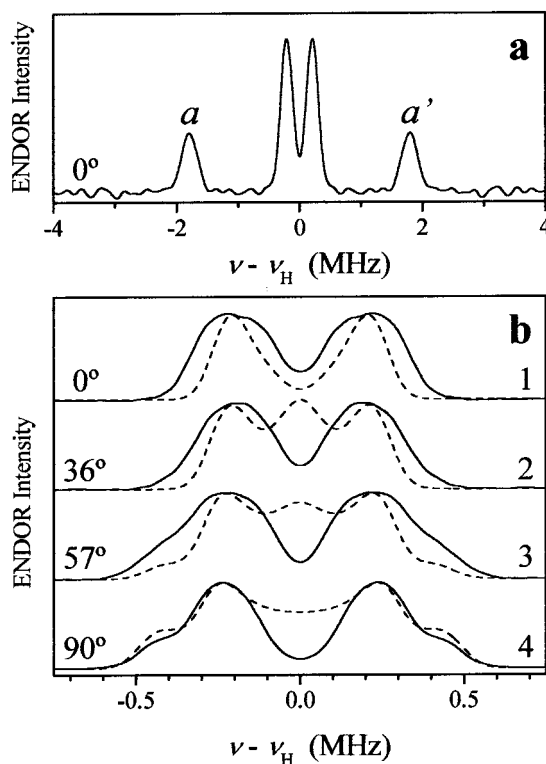

Figure 3. Experimental ^1H Mims ENDOR spectra of $[OEPFe(PhNC)_2]^+$ with CNPh-d_5. (a) Detected at $B_0 = 3550$ G. The presented trace is obtained by the summation of spectra recorded at $\tau = 325, 400,$ and 475 ns. (b) Solid traces 1 through 4, detected at $B_0 = 3550, 3325, 3125,$ and 2985 G, respectively. The traces presented are obtained by summation of spectra recorded at $\tau = 300, 375, 450, 525,$ and 600 ns. Dashed lines, ENDOR spectra simulated for a simple model with two protons at the distance $R_{FeH} = 5.7$ Å and at the angles of 0° and 20° between $\mathbf{R}_{FeH}$ and the heme plane (see text). Same as in Figure 1a, the ENDOR spectra were calculated without taking into account the Mims ENDOR intensity factor (see text). Both panels: The corresponding approximate values of θ_{BZ} are shown near each trace at the left-hand side of the figure. Solvent, CD_2Cl_2. Other experimental parameters: $\nu_{mw} = 9.44$ GHz; mw pulses, $3 \times (10$ ns); time interval between the second and third mw pulses, $T = 40$ μs; RF pulse duration (180°), 12 μs. The spectra are symmetrized with respect to the ^1H Zeeman frequency ν_H.

anisotropy in positions of lines of the protons at pyrrole β carbons would then be about 10 MHz, which contradicts our ENDOR data.

To extract information about the spin density on the *meso* carbons, the model for the anisotropic hfi tensors described in our previous work[7] has been used. The anisotropic hfi tensor is considered as consisting of two contributions, from the spin density ρ_{Fe} on the central Fe^{3+} and from the π-spin density ρ_{Cm} on the *meso* carbon nearest to a given meso proton. The total anisotropic hfi tensor (in the principal axes system) is given by

$$T_n \approx -\rho_{Fe}gg_n\beta\beta_n/hR_{FeH}^3; \quad T_{t\perp} \approx T_n - 15g\rho_{Cm};$$
$$T_{t\parallel} \approx -2T_n + 15g\rho_{Cm} \quad (2)$$

where T_n corresponds to the heme normal, and $T_{t\perp}$ and $T_{t\parallel}$ correspond to the in-plane directions being, respectively, perpendicular and parallel to radius-vector $\mathbf{R}_{FeH}$ connecting the central Fe^{3+} ion with the *meso* proton. All T values are in MHz; R_{FeH} is about 4.5 Å; g and g_n are respectively the electronic and nuclear g factors; β and β_n are the Bohr magneton and the nuclear magneton; and h is Planck's constant.

Low-Spin Iron(III) Porphyrinate Complexes

J. Phys. Chem. A, Vol. 106, No. 1, 2002 **77**

The spin density ρ_{Cm} also gives rise to the isotropic hfi constant of a *meso* proton determined by the McConnell relation:

$$a_m = Q_m \rho_{Cm} \qquad (3)$$

with $Q_m \cong -63$ MHz.[40] With the expected significant positive ρ_{Cm},[10,11] a_m is negative.

Now we can also independently deduce from the spectra shown in Figure 2a that $g_\parallel$ actually corresponds to the direction along axis Z normal to the heme plane. Indeed, using eq 2 and $R_{FeH} \approx 4.5$ Å, one can estimate $T_n \sim -1$ MHz for $g \sim 2$ and $\rho_{Fe} \sim 1$. Because the splittings of up to 6 MHz between the aa' lines in Figure 2a are much greater than $2|T_n| \sim 2$ MHz, they are mostly determined by ρ_{Cm}. It then follows from eqs 2 and 3 that in such a situation the maximal possible splitting between the aa' lines should correspond to B_0 being in the porphyrin plane and perpendicular to $\mathbf{R}_{FeH}$, and minimal possible splitting should correspond to $B_0 // \mathbf{R}_{FeH}$. From Figure 2a, one can see that the overall maximal splitting between the aa' lines is observed at $g_\perp$ (trace 4), whereas at $g_\parallel$ (trace 1), the splitting is intermediate. Because the molecular symmetry requires one of the g-tensor axes to be directed along Z, we have only two options to consider. The first one is that $g_\parallel$ corresponds to the line joining two opposite *meso* protons, and $g_\perp$ corresponds to the plane formed by Z and the line joining the two remaining opposite *meso* protons. This option, however, contradicts the experimental data because it predicts the splitting for two of the *meso* protons at $g_\parallel$ to be maximal. The remaining possibility is that $g_\perp$ corresponds to the porphyrin plane and $g_\parallel$ corresponds to Z (in other words, $g_\parallel$ is g_Z). This option agrees with all of the ENDOR spectra in Figure 2a and with the Mössbauer data.[10,11]

Simulation of the aa' lines in the ENDOR spectra in Figure 2a using eqs 2 and 3 can be used to estimate the spin densities ρ_{Fe} and ρ_{Cm}. It should be noted that in our previous work,[7] dealing with the $(d_{xy})^2(d_{xz},d_{yz})^3$ (which can also be called d_π) complexes of iron(III) porphyrins, we have assumed $\rho_{Fe} \approx 1$ and have used the ENDOR simulation to estimate the spin densities on pyrrole β carbons (which were functionally similar to ρ_{Cm} in this work). Here, however, a certain caution must be exercised with respect to ρ_{Fe} because previously reported Mössbauer data clearly showed considerably reduced hyperfine interactions of the iron nuclei in bis-isocyanide complexes, corresponding to ρ_{Fe} of 0.5−0.8, depending on the porphyrin and the axial ligands.[10,11] Also DFT calculations predict the spin density ρ_{Fe} to be considerably decreased in the d_{xy} complexes compared to the value of about 0.8 typical for the complexes with the d_π configuration.[39] A significant part of the spin density in the d_{xy} complexes is predicted to be delocalized to the four *meso* carbons,[39] three of which are rather far away from any given *meso* proton. On the basis of the above considerations and the fact that *meso* protons are closer to the central Fe^{3+} than the pyrrole protons studied in the earlier work,[7] it was felt that taking $\rho_{Fe} \approx 1$ would not be a fair assumption for the d_{xy} systems under investigation (and indeed, preliminary ENDOR simulations showed that the spectra simply could not be satisfactorily fit assuming $\rho_{Fe} = 1$). Therefore, in the simulations, both ρ_{Fe} and ρ_{Cm} were used as adjustable parameters.

The simulation has allowed the dependence of the shape of the aa' lines on the observation position in the EPR spectrum to be successfully fit. The values of ρ_{Fe} and ρ_{Cm} found from these calculations are about 0.63 and 0.06, respectively. The ENDOR spectra simulated with these spin densities are shown by dashed lines in Figure 2a. With $\rho_{Cm} \approx 0.06$, the isotropic hfi constant is $a_m \approx -3.8$ MHz.

3. Spin Densities on Pyrrole β Carbons. The central intense lines in the ^1H ENDOR spectra of $[OEPFe(PhNC)_2]^+$ (Figure 2a) are contributed by ethyl protons and phenyl protons of axial ligands. The hyperfine interactions of the ethyl protons are sensitive to the spin density on the pyrrole β carbons. To obtain pure spectra of the ethyl protons, the samples with deuterated axial ligands ($CNPh-d_5$) were used. The spectra recorded at several B_0 settings are shown in Figure 3b. The spectrum at $g_\parallel$ shows a broad doublet with an average splitting of about 0.42 MHz. The spectrum at $g_\perp$ shows a more complicated structure, with two intense lines with a splitting of about 0.48 MHz and two outer shoulders with a splitting of about 0.97 MHz.

There are two methylene and three methyl protons in each ethyl group. Depending on the rotational orientation of the ethyl group, the distance from Fe^{3+} to the methylene protons varies from about 5.6 to 6.3 Å, and the maximal angle between the heme plane and the direction from Fe^{3+} to a methylene proton is about 10°. The distance from Fe^{3+} to the methyl protons can formally vary from about 4.8 to 7.5 Å, and the maximal possible angle between the heme plane and the direction from Fe^{3+} to a methyl proton is about 20°. The minimal distance of 4.8 Å for a methyl proton, however, can hardly be realized because at this conformation of the ethyl group the methyl proton would be only about 0.5 Å away from a *meso* proton. Because all ethyl protons are close to the porphyrin plane (the angle between $\mathbf{R}_{FeH}$ and the heme plane is no greater than 20°), the ENDOR spectra can be interpreted as follows.

Two main peaks observed at $g \approx g_\perp \approx 2.26$ correspond to an effective average perpendicular component ($A_\perp \approx 0.48$ MHz) of the axial hyperfine interaction tensor of ethyl protons, and the two shoulders correspond to the parallel component ($A_\parallel \approx 0.97$ MHz). Because $A_\parallel/A_\perp \approx 2$, the isotropic hfi for the pyrrole protons is negligible, which means that the spin density on the pyrrole β carbons is about zero. The values of $A_\parallel$ and $A_\perp$ are then equal to the respective components of the anisotropic hfi $T_\parallel$ and $T_\perp$ and allow one to estimate the effective distance of about 5.7 Å from Fe^{3+}. This value of R_{FeH} was obtained in the point dipole approximation and assuming $\rho_{Fe} = 1$, which is now a reasonable estimate for ρ_{Fe}, because the ethyl protons are relatively far away from Fe^{3+} and the spin density distributed over the porphyrin plane is to be included into the effective value of ρ_{Fe}. Two peaks observed at $g \approx g_\parallel \approx 1.9$ again correspond to $T_\perp$ of ethyl protons situated at the effective distance of about 5.7 Å from Fe^{3+}.

To confirm the conclusion about nearly zero isotropic hfi made above, numerical simulations of the spectra were performed. The distributed geometry of the ethyl group (with not very well defined structural constraints imposed) and possibly not exactly zero value of the isotropic hfi constants depending on this geometry (which is essential for the very narrow width of the spectra being discussed) makes it impossible to perform any accurate fitting of such ENDOR spectra. However, the general trend in the line shapes and positions can be approximately reproduced in the calculation taking into account only the anisotropic hfi of a proton at the distance of 5.7 Å and with the angle between the heme plane and the direction from Fe^{3+} to the proton being distributed from 0 to 20°. To further simplify this model, the ENDOR spectra from two protons located at the distance $\mathbf{R}_{FeH} = 5.7$ Å and at the angles of 0 and 20° between $\mathbf{R}_{FeH}$ and the heme plane have been calculated. The simulated spectra are shown in Figure 3b by dashed lines.

For the 40 protons of the ethyl groups giving the lines with a characteristic width of about 0.3 MHz and excited by the RF pulses of length 12 μs (i.e., having the excitation width of about
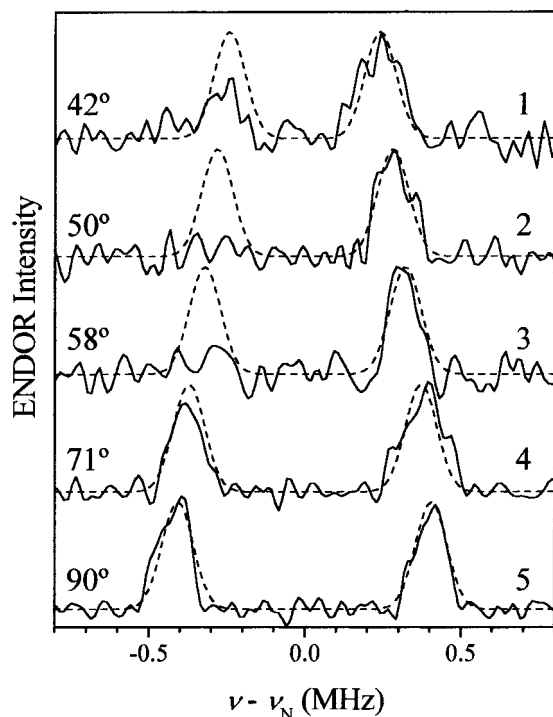
Figure 4. Solid traces 1 through 5, experimental [15]N Mims ENDOR spectra of [TPPFe(PhNC)$_2$]$^+$ in CH$_2$Cl$_2$, detected at ν_{mw} = 9.433 GHz and at B_0 = 3268, 3218, 3168, 3108, and 3068 G, respectively. The corresponding approximate values of θ_{BZ} are shown near each trace at the left-hand side of the figure. Other experimental parameters: mw pulses, 3 × (15 ns); time interval between the second and third mw pulses, T = 70 μs; RF pulse duration (90°), 40 μs. The traces shown represent the differences between the spectra for the samples with [15]N- and ^{14}N-substituted isocyanide ligands. Each of the above spectra was obtained by summation of spectra recorded at τ = 510, 560, 590, 640, and 690 ns. Dashed lines, ENDOR spectra simulated for an ^{15}N with a_{iso} = 0.62 MHz and $T_\perp$ = 0.2 MHz, without taking into account the Mims ENDOR intensity factor.

0.1 MHz), the situation of simultaneous excitation of many protons (for each unpaired electron) will be realized, with all of the complications and (practically unpredictable) distortions of the blind spot behavior discussed in ref 41. Therefore, the ENDOR spectra in Figure 3b were calculated without taking into account the Mims ENDOR intensity factor $1 - \cos(2\pi A\tau)$.[34] This resulted in a large ENDOR intensity in the simulated spectra for the hfi values approaching zero (especially in the dashed traces 2 and 3), whereas in the experimental spectra, the lines corresponding to $A \rightarrow 0$ were suppressed by a blind spot.

4. Nitrogens of the Isocyanide Ligands. To obtain information on the hyperfine interactions of the nitrogens in the axial ligands, Mims ENDOR spectra of [TPPFe(PhNC)$_2$]$^+$ were recorded for the samples with [15]N- and ^{14}N-substituted isocyanides and subtracted from one another. The resulting spectra contained only the lines due to ^{15}N in the isocyanide ligands (see Figure 4 where the difference spectra obtained at different B_0 are shown). The lines due to the isocyanide [14]N (which should have been manifested as dips in the difference spectra) were not observed, probably because of their weakness caused by strong broadening by the nuclear quadrupole interaction (nqi).

At $g_\perp$, two lines are observed situated symmetrically with respect to the nitrogen Zeeman frequency ν_N, with a splitting between them of about 0.8 MHz. As B_0 increases toward the $g_{||}$ region, the splitting between these lines decreases, whereas the width of the lines remains unchanged. Because, for an axial g

tensor, any B_0 corresponds to a unique angle θ_{BZ}, the constant line width indicates that, as expected, the hfi tensor for ^{15}N is (within our accuracy) axially symmetric, with the main axis directed along Z. The asymmetry in line intensities in the experimental spectra is, most probably, caused by the implicit TRIPLE effect.[38]

We have not been able to trace the decrease of the line splitting across the whole EPR spectrum because of the weakness of the ^{15}N ENDOR effect (about 6%) and decrease of the EPR signal as the magnetic field approaches that of $g_{||}$. In addition, the decrease in the line splitting required ever increasing values of τ to be used, which led to a further decrease of the available ESE signal intensity. However, the observed dependence of the splitting on B_0 (or θ_{BZ}) was sufficient to determine the hfi parameters of these nitrogens. The isotropic and anisotropic hfi parameters found are $|a_{iso}|$ = 0.62 MHz and $|T_\perp|$ = 0.2 MHz (scaled to g = 2), where a_{iso} and $T_\perp$ are of the same sign. Dashed traces in Figure 4 show the ENDOR spectra simulated with these parameters. With this type of spectra, taking into account the Mims ENDOR intensity factor was not necessary.

5. Carbons of the Isocyanide Ligands. To obtain the information on the spin density delocalization to the carbons of the −NC groups of the isocyanide ligands in [TPPFe-(PhNC)$_2$]$^+$, these carbons were substituted with [13]C. The ^{13}C lines in ENDOR and ESEEM spectra were identified from comparison with the spectra obtained from the ^{12}C-containing sample. As will become clear shortly, the situation involved with detecting ^{13}C lines was more complicated than found for other nuclei.

On the basis of axial symmetry of the complex structure and its g tensor, it was anticipated that the hfi tensor of ^{13}C would also be axial, with the principal axes of this nucleus being collinear to those of the g tensor (as observed for the ^{15}N in the isocyanide groups). Therefore, at the canonical orientations of the g tensor (coinciding with the canonical orientations of the hfi tensor and corresponding to the turning points in the EPR spectrum), no ^{13}C ESEEM was expected. Consequently, we used pulsed ENDOR to detect ^{13}C at $g_\perp$.

From preliminary measurements, it became clear that in Mims ENDOR spectra the observation of the only identifiable ^{13}C line was obscured by the more intense ^{1}H transitions induced by the second and third RF harmonics (caused by the nonlinearities of the RF amplifier at the high RF power used). Therefore, it was necessary to use Davies ENDOR, which, with a 180° mw pulse of 100 ns, shows much smaller ^{1}H ENDOR effect both in the main (first) harmonic and in the higher harmonics.

The Davies ENDOR spectra detected at ν_{mw} = 9.441 GHz and B_0 = 3083 G (at $g_\perp$) in the samples with [13]CNPh and [12]CNPh ligands are shown by respectively the solid and dashed traces 1 in Figure 5. The only observable line of ^{13}C that can be identified from comparison of these spectra is shaded in solid trace 1. It is not clear from this single measurement whether this line is the high- or low-frequency line of the nuclear transition doublet. At this magnetic field, the Zeeman frequency of ^{13}C, ν_C, is equal to 3.3 MHz. Therefore, if the line observed is the low-frequency one, it corresponds to the strong interaction case and its frequency is $\nu = |A|/2 - \nu_C$. If this line is the high-frequency component, it corresponds to the weak coupling case and its frequency is $\nu = |A|/2 + \nu_C$.

To decide which of these situations is the case, we have performed the Davies ENDOR experiment at ν_{mw} = 11.318 GHz and B_0 = 3687 G (this setting also corresponds to $g_\perp$). The spectra obtained are shown by solid ([13]CNPh) and dashed
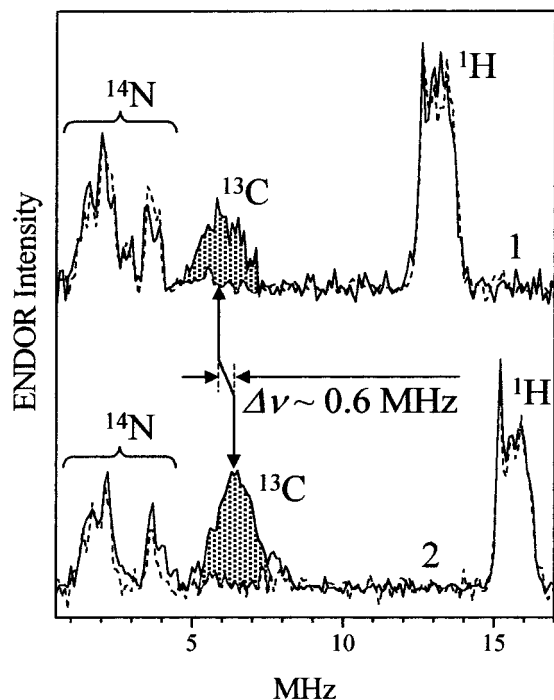
Low-Spin Iron(III) Porphyrinate Complexes

J. Phys. Chem. A, Vol. 106, No. 1, 2002 **79**

Figure 5. Traces 1 and 2, experimental Davies ENDOR spectra of $[TPPFe(PhNC)_2]^+$ in CH_2Cl_2, detected at $\nu_{mw} = 9.441$ GHz and $B_0 = 3083$ G and at $\nu_{mw} = 11.318$ GHz and $B_0 = 3687$ G, respectively, for the samples with ^{13}CNPh (solid traces) and ^{12}CNPh (dashed traces). These ν_{mw}/B_0 settings correspond to $\theta_{BZ} \approx 90°$. Other experimental parameters: mw pulses, 100 (180°), 50 (90°), and 100 ns (180°); time interval between the first and second mw pulses, $T = 60$ μs; RF pulse duration (180°), 30 μs; time interval between the second and third mw pulses, $\tau = 600$ ns. The assignment of various lines to different nuclei is shown in the spectra. The ^{13}C line is shaded.
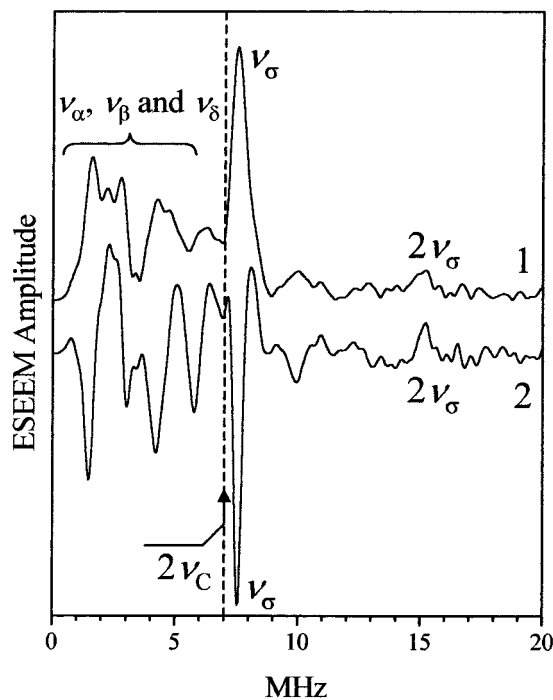

Figure 6. Traces 1 and 2 are respectively amplitude and cosine Fourier transforms of quotient primary ESEEM obtained by division of the primary ESEEM recorded for the sample of $[TPPFe(PhNC)_2]^+$ with ^{13}CNPh by that recorded for the sample with ^{12}CNPh. Solvent, CH_2-Cl_2. Experimental conditions: $\nu_{mw} = 9.436$ GHz, $B_0 = 3268$ G ($\theta_{BZ} \approx 42°$), and mw pulses of 10 ns duration. The most intense and unambiguous line is the sum combination harmonic of ^{13}C ($\nu_\sigma = 7.52$ MHz). The expected positions of fundamental lines ν_α and ν_β, the difference combination line ν_δ, and the $2\nu_\sigma$ line (which appears because two ^{13}C nuclei contribute to the ESEEM) are also shown in the spectra.

(^{12}CNPh) traces 2 in Figure 5. Comparing traces 1 and 2, one can see that the ^{13}C line has shifted to higher frequencies by about 0.6 MHz, which is approximately equal to the change of the Zeeman frequency of ^{13}C ν_C, $\Delta\nu_C \approx 0.65$ MHz. This experiment shows clearly that the observed line is actually the high-frequency line of the ^{13}C doublet, and the single observable ^{13}C signal of the isocyanide ligands corresponds to the weak interaction case. From the ENDOR line positions (≈ 5.9 MHz in trace 1 and ≈ 6.5 MHz in trace 2) and the ν_C values (≈ 3.3 MHz in trace 1 and ≈ 3.95 MHz in trace 2), the hfi constant $|A_\perp| \approx 5.15 \pm 0.05$ MHz corresponding to the line maxima can be estimated.

Unfortunately, because of a dramatic decrease in ESE intensity, we have not been able to detect the Davies ENDOR spectra at g values other than those close to $g_\perp$. Therefore, to obtain information on the anisotropic hfi, ESEEM experiments were employed. For the axially symmetric hfi tensor coaxial with the g tensor, the maximal ESEEM intensity is expected at $\theta_{BZ} \approx 45°$. At such an orientation of B_0 ($\nu_{mw} = 9.436$ GHz, $B_0 = 3268$ G, and $\theta_{BZ} \approx 42°$), the division of the primary ESEEM traces recorded for the ^{13}C- and ^{12}C-containing samples by one another has allowed the unambiguous detection of the ^{13}C sum combination line ν_σ ($\nu_\sigma = 7.52$ MHz, see Figure 6). This line is shifted from $2\nu_C \approx 7$ MHz by about 0.5 MHz to higher frequencies. Using the expression derived in ref 42, the anisotropic hfi of the isocyanide ^{13}C can then be estimated as $|T_\perp| \approx 1.75$ MHz (scaled to $g = 2$). As for the lines with the lower frequencies in the primary ESEEM spectrum, it is not clear at this stage whether they mostly belong to the carbon ^{13}C or they are mostly the remainder of the extremely intense ^{14}N lines crowding this spectral region. (Such a remainder can

be observed because of nonperfect background suppression by the phase cycling.)

To obtain the sign of $T_\perp$ (relative to that of the isotropic hfi constant a_{iso}), the ^{13}C fundamental lines must be detected and the change in their position must be traced across the EPR spectrum. For a_{iso} and $T_\perp$ of the same sign, the fundamental lines should approach each other as B_0 is shifted toward $g_\parallel$, whereas for a_{iso} and $T_\perp$ of opposite signs, the splitting between the lines should increase. To accomplish the above task, two-dimensional (2D) ESEEM techniques seemed to be the most appropriate. Therefore, hyperfine sublevel correlation (HY-SCORE)[43] and refocused primary (RP) ESEEM[44] measurements were performed at magnetic field positions corresponding to $\theta_{BZ} \approx 55°$ (close to the magic angle, where the splitting should be close to the isotropic hfi constant) and also at 32°. It was found that HYSCORE did not perform well at $\theta_{BZ} \approx 55°$ because only a very limited set of time intervals τ provided signal intensity sufficient for the measurements. On the other hand, relatively long electronic transverse relaxation time T_2 in these systems allowed the RP ESEEM spectrum to be obtained easily, with a resolution sufficient to identify the positions of the ^{13}C lines. The RP ESEEM spectrum for $\theta_{BZ} \approx 55°$ is presented in Figure 7a. The assignments of various correlation lines are also shown in the figure.

The (α,β) and (β,α) ^{13}C correlation lines are evident at the frequencies of (2.3,5.3) and (5.3,2.3) MHz. The lines on the main diagonal at (2.3,2.3) and (5.3,5.3) MHz are the (α,α) and (β,β) correlations that are normally not observable in the spectra of disordered systems because of the self-suppression effect.[44] Here, however, because of the orientational selectivity and the axiality of the anisotropic hfi, these lines do not extend
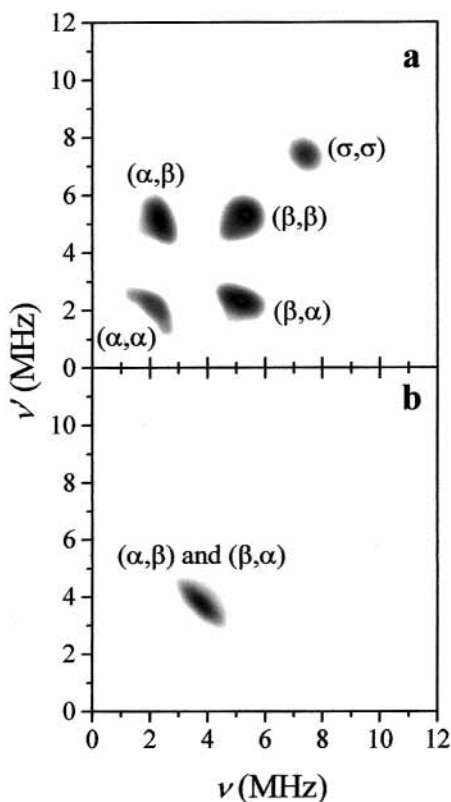
Figure 7. (a) (++) quadrant of the spectrum of quotient RP ESEEM obtained by division of the RP ESEEM recorded for the sample of [TPPFe(PhNC)$_2$]$^+$ with ^{13}CNPh by that recorded for the sample with ^{12}CNPh. The spectrum is symmetrized with respect to the main diagonal. Solvent, CH$_2$Cl$_2$. Experimental conditions: $\nu_{mw} = 9.4485$ GHz, $\boldsymbol{B}_0 = 3183$ G ($\theta_{BZ} \approx 55°$), and all mw pulses of 15 ns duration. The assignments of the most intense ^{13}C lines are shown in the figure. (b) (++) quadrant of the HYSCORE spectrum obtained as a difference between the spectra of [TPPFe(PhNC)$_2$]$^+$ with ^{12}CNPh and ^{13}CNPh. The spectrum is symmetrized with respect to the main diagonal. Solvent, CH$_2$Cl$_2$. Experimental conditions: $\nu_{mw} = 9.4485$ GHz, $\boldsymbol{B}_0 = 3333$ G ($\theta_{BZ} \approx 32°$), $\tau = 380$ ns, and all mw pulses of 15 ns duration.

significantly along the main diagonal and are clearly seen. The extension of the (α,α) feature across the main diagonal may be caused by a contribution of ^{14}N$-^{13}$C combination lines that were not completely suppressed by division of the ESEEM traces (because this is an orientationally disordered situation). The line at (7.48,7.48) MHz is the (σ,σ) correlation line, which is also shifted from the exact ($2\nu_C,2\nu_C$) position.

At $\theta_{BZ} \approx 32°$, on the other hand, the situation was favorable for HYSCORE, and a clear ^{13}C spectrum was obtained, which is shown in Figure 7b. One can see that at $\theta_{BZ} \approx 32°$ the (α,β) and (β,α) ^{13}C correlation lines have nearly converged at the main diagonal.

The fact that the splitting between the fundamental lines of ^{13}C decreases with decreasing θ_{BZ} indicates that a_{iso} and $T_\perp$ are of the same sign. One can then estimate a_{iso} from the value of $|A_\perp| \approx 5.15$ MHz found from the ENDOR spectra in Figure 5, $|a_{iso}| = |A_\perp| - |T_\perp| \approx 3.2$ MHz. Similarly, a_{iso} can be found from the fundamental frequencies observed in Figure 7a ($\nu_\alpha \approx 2.3$ MHz and $\nu_\beta \approx 5.3$ MHz) and using the fact that $\theta_{BZ} \approx 55°$ virtually equals to the magic angle: $|a_{iso}| = (\nu_\beta{}^2 - \nu_\alpha{}^2)/(2\nu_C) \approx 3.3$ MHz.

With $|a_{iso}| \approx 3.2-3.3$ MHz and $|T_\perp| \approx 1.75$ MHz (scaled to $g = 2$), the splitting between the fundamental lines expected at $\theta_{BZ} \approx 32°$ is about 1.2 MHz or somewhat smaller than the line width (about 1.6 MHz). Therefore these lines are not resolved at $\theta_{BZ} \approx 32°$ (see Figure 7b). At $\theta_{BZ} \approx 0°$ ($g \approx g_\| \approx 1.91$) the
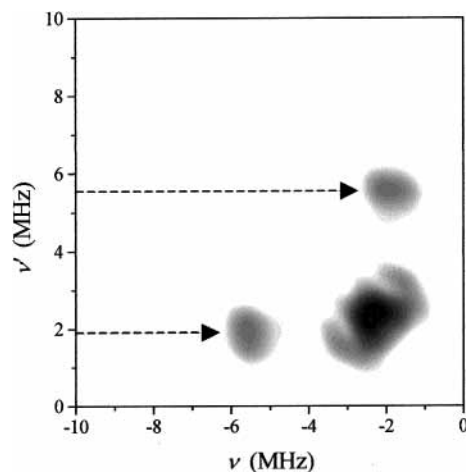

Figure 8. ($-+$) quadrant of the RP ESEEM spectrum of [TPPFe-(PhNC)$_2$]$^+$ with natural abundance of all isotopes. The spectrum is symmetrized with respect to the antidiagonal. Solvent, CH$_2$Cl$_2$. Experimental conditions: $\nu_{mw} = 9.4485$ GHz, $\boldsymbol{B}_0 = 3183$ G ($\theta_{BZ} \approx 55°$), and all mw pulses of 15 ns duration. The arrows show the $\Delta m = 2$ lines of pyrrole ^{14}N.

expected splitting is less than 0.2 MHz, which explains our failure to observe the ^{13}C lines by pulsed ENDOR at $g_\|$ (the optimal duration of the 180° mw pulse for such small splitting would be unrealistically long, greater than 3.5 μs).

6. Pyrrole Nitrogens. While studying [TPPFe(PhNC)$_2$]$^+$ with ^{13}C-enriched axial ligands, we obtained the HYSCORE and RP ESEEM spectra at several positions across the EPR spectrum. The ($-+$) quadrant of some of these spectra (particularly, the RP ESEEM ones) contained readily identifiable $\Delta m = 2$ transitions of the pyrrole nitrogens. As an example, the ($-+$) quadrant of the RP ESEEM spectrum obtained at $\nu_{mw} = 9.4485$ GHz and $\boldsymbol{B}_0 = 3183$ G ($\theta_{BZ} \approx 55°$) is shown in Figure 8. From the frequencies $\nu_1 \approx 1.9$ MHz and $\nu_2 \approx 5.6$ MHz of the $\Delta m = 2$ transitions of pyrrole nitrogens seen in this spectrum (marked by arrows), one can easily estimate the average secular component of the hfi coupling at this θ_{BZ}:[45]

$$A \approx \frac{\nu_2{}^2 - \nu_1{}^2}{8\nu_N} \qquad (4)$$

where ν_N is the Zeeman frequency of ^{14}N in the given magnetic field. The obtained value is $A \approx 3.5$ MHz. A similar hfi value (about 3.4 MHz) was obtained at $\theta_{BZ} \approx 42°$ ($\boldsymbol{B}_0 = 3268$ G). At other $\boldsymbol{B}_0$ settings, where HYSCORE was used, the $\Delta m = 2$ transitions were less pronounced and somewhat corrupted by other lines (combinations of $\Delta m = 1$ transitions), probably because of inadequate values of the time interval τ. Still, from approximate values of frequencies of the $\Delta m = 2$ lines the whole range of variation of A could be estimated as no greater than 3.3 ± 0.5 MHz, indicating that there is little anisotropy in the hfi values.

Discussion

In the previous section, the hfi parameters for various ligand nuclei in the [TPPFe(PhNC)$_2$]$^+$ and [OEPFe(PhNC)$_2$]$^+$ complexes have been determined. Here we wish to discuss their origin and the differences from the Fe(III) porphyrin complexes having the $(d_{xy})^2(d_{xz},d_{yz})^3$ or d_π configuration.

The hfi parameters for the *meso* protons are already cast in terms of spin densities on *meso* carbons, ρ_{Cm}, and on the central Fe^{3+} ion, ρ_{Fe}. The value $\rho_{Cm} \approx 0.06$ found in this work agrees

Low-Spin Iron(III) Porphyrinate Complexes

J. Phys. Chem. A, Vol. 106, No. 1, 2002 **81**

reasonably well with $\rho_{Cm} \approx 0.085$ estimated from the DFT calculations.[39] This value is essentially nonzero, which contrasts with the situation in complexes with the d_π orbital configuration.[39] The value $\rho_{Fe} \approx 0.63$ estimated in this work correlates with $\rho_{Fe} \approx 0.66$ estimated from Mössbauer spectra of [TPPFe-(t-BuNC)$_2$]$^+$,[10] 0.80 for [OEPFe(t-BuNC)$_2$]$^+$,[10] and 0.5–0.75 from spectra of [TPPFe(2,6-XylylNC)$_2$]$^+$ [11] and its *p*- and *m*-TTP analogues, as well as $\rho_{Fe} \approx 0.46$ obtained from DFT calculations,[39] and is significantly lower than that in the d_π complexes. One has to take into account, however, that the value estimated herein includes some contributions from the spin density delocalized into the porphyrin π system (mainly the pyrrole nitrogens) and axial ligands (mainly the carbons of CN groups) and only approximately reflects the actual spin population of the d_{xy} orbital. The fact that $\rho_{Fe} + 4\rho_{Cm} \approx 0.87$ ($\neq 1$) may be explained by two factors. First, as mentioned, the effective ρ_{Fe} is actually distributed over several atoms (although it is mostly localized on Fe), but its contribution to the anisotropic hfi is calculated using a point dipole model (T_n in eq 2), which might lead to a slight underestimation of ρ_{Fe}. Second, apart from *meso* carbons (that bear ρ_{Cm}) and pyrrole nitrogens and CN carbons (that contribute to ρ_{Fe}), there are 28 other carbons and two nitrogens in the [OEPFe(PhNC)$_2$]$^+$ complex. Very small, and practically undetectable, spin densities delocalized to all of these atoms may account in total for the apparent spin density deficit of 0.13 (with 30 atoms, the required average spin density per atom is only about 0.004).

The spin density on the pyrrole β carbons is found to be negligible, and thus, the data for the spin density distribution over the porphyrin macrocycle confirm the accuracy of the theoretical calculations. There is, therefore, good reason to believe that the general picture given by the DFT calculation[39] is accurate and the spin density on the pyrrole α carbons is also negligible.

The hyperfine coupling constants of the pyrrole nitrogens in d_π complexes of iron porphyrins ligated by imidazoles are, on average, $A \approx 5.5 \pm 0.5$ MHz, depending on the orientation of the $\boldsymbol{B}_0$ vector relative to the complex.[46] Such strong and essentially isotropic hfi cannot be explained by spin density in the π orbital of ^{14}N because in that case the anisotropic and isotropic contributions to the hfi would be comparable.[47] The large isotropic contribution to the ^{14}N hfi obviously comes from polarization of the Fe–N σ bond that contributes very little to the hfi anisotropy (which in this case is mostly governed by the spin density on the central Fe^{3+}).

The DFT calculations predict for the d_{xy} complexes a significant increase of π-spin density ρ_N on the pyrrole nitrogens compared with that in the d_π complexes.[39] However, the hfi constants on the pyrrole nitrogens of [TPPFe(PhNC)$_2$]$^+$ are actually about 1.5 times *smaller* than those in the bis-(imidazole) ligated iron(III) porphyrins.[46] Again, the estimated values of isotropic and anisotropic contributions to the hfi are not commensurate, suggesting a significant σ contribution to the isotropic hfi. Thus, the hfi data on pyrrole nitrogens cannot be straightforwardly cast in terms of the π-spin density, and therefore, we did not pursue the detailed mapping of the ^{14}N transitions across the EPR spectrum.

The anisotropic hfi values for the ^{13}C and ^{15}N nuclei of the isocyanide ligands (scaled to $g = 2$) are about 1.75 and 0.2 MHz, respectively. With $\rho_{Fe} \approx 0.63$ and the distances from the iron atom to the ligand carbon and nitrogen (about 1.94 and 3.1 Å, respectively[10,11]), one can easily estimate the ρ_{Fe} contributions to the anisotropic hfi to be about 1.73 MHz for ^{13}C and about 0.17 MHz for ^{15}N, which are very close to the

experimental values. The above coincidence may indicate that the π-spin density delocalization to the isocyanide group is negligible (as would be expected based on orbital symmetry considerations) and the isotropic hfi constants are determined solely by the polarization of the Fe–C–N σ-bonds.

The alternative explanation would be to assume the total π-spin densities in the p orbitals of C and N to be about 0.14 and 0.01, respectively. Together with $\rho_{Fe} \approx 0.63$, such π-spin densities (distributed equally between the two unhybridized p orbitals of each of these atoms) would also produce the anisotropic hfi tensors of isocyanide ^{13}C and ^{15}N with the experimental values of $T_\perp$ (though now $T_\perp$ will have the sign opposite to that determined by ρ_{Fe} alone). It appears that in such a model the π-spin density on the isocyanide carbon is unreasonably large, and therefore, this model is hardly reasonable for this atom. For nitrogens, on the other hand, the possibility of the estimated spin density delocalization cannot be ruled out.

Conclusions

In this work, pulsed ENDOR and ESEEM spectroscopies have been used to characterize two representatives of iron–porphyrin complexes with d_{xy} orbital configuration, [TPPFe-(PhNC)$_2$]$^+$ and [OEPFe(PhNC)$_2$]$^+$. The spin density distribution in the porphyrin π system was obtained, with major spin density ($\sim$0.06) being delocalized to *meso* carbon atoms. The spin density on pyrrole β carbons was found to be negligible. The upper limit for spin density on Fe^{3+} was estimated to be about 0.63. The hfi constants on pyrrole nitrogens (on average, $\sim$3.3 MHz) were also evaluated. The overall spin density distribution obtained was found to be in agreement with that estimated theoretically from DFT calculations[33] and different from the distribution known for the complexes with d_π orbital configuration. The latter complexes show negligible spin density on *meso* carbons, noticeable spin density on pyrrole β carbons (up to 0.015), greater spin density on Fe^{3+} ($\sim$0.8), and smaller spin density (though larger hfi constants) on the pyrrole nitrogens.[46]

The results of this work will be helpful for understanding high-resolution EPR data for biological complexes that may have the d_{xy} ground state, including low-spin iron(III) isobacteriochlorins such as the siroheme center of sulfite reductase.[18,19]

References and Notes

(1) Safo, M. K.; Gupta, G. P.; Walker, F. A.; Scheidt, W. R. *J. Am. Chem. Soc.* **1991**, *113*, 5497.

(2) Safo, M. K.; Gupta, G. P.; Watson, C. T.; Simonis, U.; Walker, F. A.; Scheidt, W. R. *J. Am. Chem. Soc.* **1992**, *114*, 7066.

(3) Raitsimring, A. M.; Borbat, P.; Shokhireva, T. Kh.; Walker, F. A. *J. Phys. Chem.* **1996**, *100*, 5235.

(4) Raitsimring, A. M.; Walker, F. A. *J. Am. Chem. Soc.* **1998**, *120*, 991.

(5) Astashkin, A. V.; Raitsimring, A. M.; Walker, F. A. *Chem. Phys. Lett.* **1999**, *306*, 9.

(6) Schünemann, V.; Raitsimring, A. M.; Benda, R.; Trautwein, A. X.; Shokhireva, T. Kh.; Walker, F. A. *J. Biol. Inorg. Chem.* **1999**, *4*, 708.

(7) Astashkin, A. V.; Raitsimring, A. M.; Walker, F. A. *J. Am. Chem. Soc.* 2001, *123*, 1905.

82 *J. Phys. Chem. A, Vol. 106, No. 1, 2002*

Astashkin et al.

(8) Simonneaux, G.; Hindré, F.; Le Plouzennec, M. *Inorg. Chem.* **1989**, *28*, 823.

(9) Safo, M. K.; Walker, F. A.; Raitsimring, A. M.; Walters, W. P.; Dolata, D. P.; Debrunner, P. G.; Scheidt, W. R. *J. Am. Chem. Soc.* **1994**, *116*, 7760.

(10) Walker, F. A.; Nasri, H.; Turowska-Tyrk, I.; Mohanrao, K.; Watson, C. T.; Shokhirev, N. V.; Debrunner, P. G.; Scheidt, W. R. *J. Am. Chem. Soc.* **1996**, *118*, 12109.

(11) Simonneaux, G.; Schünemann, V.; Morice, C.; Carel, L.; Toupet, L.; Winkler, H.; Trautwein, A. X.; Walker, F. A. *J. Am. Chem. Soc.* **2000**, *122*, 4366.

(12) Wołowiec, S.; Latos-Graóyński, L.; Mazzanti, M.; Marchon, J.-C. *Inorg. Chem.* **1997**, *36*, 5761.

(13) Wojaczyński, J.; Latos-Grażyński, L.; Głowiak, T. *Inorg. Chem.* **1997**, *36*, 6299.

(14) Nakamura, M.; Ikeue, T.; Fujii, H.; Yoshimura, T. *J. Am. Chem. Soc.* **1997**, *119*, 6284.

(15) Wołowiec, S.; Latos-Grażyński, L.; Toronto, D.; Marchon, J.-C. *Inorg. Chem.* **1998**, *37*, 724.

(16) Nakamura, M.; Ikue, T.; Fujii, H.; Yoshimura, T.; Tajima, K. *Inorg. Chem.* **1998**, *37*, 2405.

(17) Ikue, T.; Ohgo, Y.; Saitoh, T.; Nakamura, M.; Fujii, H.; Yokoyama, M. *J. Am. Chem. Soc.* **2000**, *122*, 4068.

(18) Crane, B. R.; Siegel, L. M.; Getzoff, E. D. *Science* **1995**, *270*, 59.

(19) Kaufman, J.; Siegel, L. M.; Spicer, L. D. *Biochemistry* **1993**, *32*, 8782.

(20) Hori, H. *Biochim. Biophys. Acta* **1971**, *251*, 227.

(21) Mailer, C.; Taylor, C. P. S. *Can. J. Biochem.* **1972**, *50*, 1048.

(22) Devaney, P. W. Ph.D. Dissertation, University of Illinois, 1980.

(23) Byrn, M. P.; Katz, B. A.; Keder, N. L.; Levan, K. R.; Magurany, C. J.; Miller, K. M.; Pritt, J. W.; Strouse, C. E. *J. Am. Chem. Soc.* **1983**, *105*, 4916.

(24) Quinn, R.; Valentine, J. S.; Byrn, M. P.; Strouse, C. E. *J. Am. Chem. Soc.* **1987**, *109*, 3301.

(25) Soltis, S. M.; Strouse, C. E. *J. Am. Chem. Soc.* **1988**, *110*, 2824.

(26) Inniss, D.; Soltis, S. M.; Strouse, C. E. *J. Am. Chem. Soc.* **1998**, *110*, 5644.

(27) Adler, A. D.; Longo, F. R.; Finarelli, J. D.; Goldmacher, J.; Assour, J.; Korsakoff, L. *J. Org. Chem.* **1967**, *32*, 476.

(28) Walker, F. A.; Balke, V. L.; McDermott, G. A. *Inorg. Chem.* **1982**, *21*, 3342.

(29) Walker, F. A.; Balke, V. L.; McDermott, G. A. *J. Am. Chem. Soc.* **1982**, *104*, 1569.

(30) Vlietstra, E. J.; Zwikker, J. W; Nolte, R. J. M.; Drenth, W. *Recl. J. R. Neth. Chem. Soc.* **1982**, *101*, 460.

(31) Obrecht, R.; Herrmann, R.; Ugi, I. *Synthesis* **1985**, *4*, 400.

(32) Borbat, P. P.; Raitsimring, A. M. *Abstracts of 36th Rocky Mountain Conference on Analytical Chemistry*; Denver, CO, 1994; p 94.

(33) Astashkin, A. V.; Mader Cosper, M.; Raitsimring, A. M.; Enemark, J. H. *Inorg. Chem.* **2000**, *9*, 4989.

(34) Mims, W. B. *Proc. R. Soc. London* **1965**, *283*, 482.

(35) Davies, E. R. *Phys. Lett. A* **1974**, *47*, 1.

(36) Grupp, A.; Mehring, M. Pulsed ENDOR Spectroscopy in Solids. In *Modern Pulsed and Continuous Wave Electron Spin Resonance*; Kevan, L., Bowman, M., Eds.; Wiley: New York, 1990, p 195.

(37) Thomann, H.; Bernardo, M. Pulsed Electron Nuclear Multiple Resonance Spectroscopic Methods for Metalloproteins and Metalloenzymes. In *Methods in Enzymology*; Riordan, J. F., Vallee, B. L., Eds.; Academic Press: San Diego, CA, 1993; Vol. 227, p 118.

(38) Doan, P. E.; Nelson, M. J.; Jin, H.; Hoffman, B. M. *J. Am. Chem. Soc.* **1996**, *118*, 7014.

(39) Ghosh, A.; Gonzalez, E.; Vangberg, T. *J. Phys. Chem. B* **1999**, *103*, 1363.

(40) McConnell, H. M.; Dearman, H. H. *J. Chem. Phys.* **1958**, *28*, 51.

(41) Astashkin, A. V.; Kawamori, A. *J. Magn. Reson.* **1998**, *135*, 406.

(42) Astashkin, A. V.; Dikanov, S. A.; Tsvetkov, Yu. D. *Chem. Phys. Lett.* **1987**, *136*, 204.

(43) Höfer, P.; Grupp, A.; Nebenführ, H.; Mehring A. *Chem. Phys. Lett.* **1986**, *132*, 279.

(44) Astashkin, A. V.; Raitsimring, A. M. *J. Magn. Reson.* **2000**, *143*, 280.

(45) Astashkin, A. V.; Dikanov, S. A.; Tsvetkov, Yu. D. *J. Struct. Chem.* **1985**, *26*, 363.

(46) Scholes, C. P.; Falkowski, K. M.; Chen, S.; Bank, J. *J. Am. Chem. Soc.* **1986**, *108*, 1660.

(47) Carrington, A.; McLachlan, A. D. *Introduction to Magnetic Resonance with Applications to Chemistry and Chemical Physics*; Harper and Row Publishers: NewYork, 1967.